

WHOLE BODY DIFFUSION MRI VS PET CT

ΕΠΙΣΤΗΜΟΝΙΚΗ ΟΜΑΔΑ:
Σ.Ι.Τρακάδας, Σ.Λάχανης, Α.Παπαδόπουλος

Αγαπητέ συνάδελφε ,

οι τεχνολογικές εξελίξεις στην μαγνητική τομογραφία προσφέρουν σημαντικές νέες δυνατότητες στην διάγνωση, την σταδιοποίηση και την παρακολούθηση των ογκολογικών ασθενών. Σκοπός της επικοινωνίας μαζί σας είναι η ενημέρωσή σας, ώστε να επιλέξετε την καταλληλότερη διαγνωστική μέθοδο για τους ασθενείς σας.

Η τεχνική **ολόσωμης διάχυσης (whole body diffusion)** είναι πλέον διαθέσιμη στους τελευταίους γενιάς μαγνητικούς τομογράφους σε κλινικό επίπεδο.

Η φυσική της βάση είναι η μελέτη της τυχαίας κίνησης των πρωτονίων του νερού μέσα σε ένα περιβάλλον. Ιστοί έντονα κυτταροβριθείς, όπως είναι οι καρκινικοί ιστοί, εμφανίζουν περιορισμένη διάχυση και διαχωρίζονται εύκολα και με μεγάλη αντίθεση από τους φυσιολογικούς ιστούς.

Σε μια συνεδρία γίνεται έλεγχος ολοκλήρου του σώματος από τον εγκέφαλο έως την μεσότητα των μηρών. Ο χρόνος της εξέτασης είναι μόλις **30 min**.

Η τεχνική **επιτυγχάνει ακριβή σταδιοποίηση** των ογκολογικών ασθενών αναδεικνύοντας την πρωτοπαθή εστία, λεμφαδενικές διογκώσεις και μεταστάσεις .

Χάρη στην ευελιξία της μαγνητικής τομογραφίας τα επιμέρους ευρήματα είναι δυνατόν να διευκρινιστούν περαιτέρω, όσον αφορά την εντόπιση ή τον χαρακτηρισμό τους, με κλασσικές τομές με ή χωρίς την ε/φ χορήγηση παραμαγνητικής ουσίας ανάλογα με την ένδειξη.

Η τεχνική επιτρέπει επίσης, την παρακολούθηση των ογκολογικών ασθενών και εκτιμά την ανταπόκριση των νεοπλασματικών εστιών στην εφαρμοζόμενη θεραπεία με βάση τις μεταβολές στις τιμές του συντελεστή διάχυσης.

Αν και το φυσιολογικό υπόβαθρο είναι διαφορετικό οι εικόνες και οι πληροφορίες είναι παρόμοιες με αυτές του PET/CT, **σε αρκετές μελέτες που έχουν δημοσιευθεί , η ευαισθησία, η ειδικότητα και η ακρίβεια των δύο μεθόδων είναι παρόμοια.**

Αφορούν ασθενείς με διάφορες νεοπλασματικές καταστάσεις, όπως λεμφώματα, μικροκυτταρικό και μη μικροκυτταρικό νεόπλασμα του πνεύμονος, νεοπλάσματα του γαστρεντερικού, νεοπλάσματα του μαστού, μελάνωμα κ.λπ.

Η τεχνική ολόσωμης διάχυσης αποτελεί αυτήν την στιγμή την **μοναδική αξιόπιστη** εναλλακτική μέθοδο του PET/CT επιτρέποντας σε μία μόνο συνεδρία ακριβή σταδιοποίηση των ογκολογικών ασθενών .Ταυτόχρονα εμφανίζει αρκετά **πλεονεκτήματα**, όπως είναι η **διαθεσιμότητα**, το **κόστος**, ο **χρόνος εξέτασης** και το σημαντικότερο όλων: **χωρίς ιοντίζουσα ακτινοβολία καθιστώντας δυνατό, ο ασθενής να υπόκειται σε τακτικότερους επανελέγχους.**

Πλεονεκτήματα επίσης είναι, η **δυνατότητα ανίχνευσης μικρότερων νεοπλασματικών εστιών**, λόγω της υψηλότερης διακριτικής ικανότητας και η καλύτερη διερεύνηση νεοπλασμάτων με χαμηλή συγκέντρωση 18F-FDG στο PET/CT όπως μερικά νεοπλάσματα του θυρεοειδούς, ηπατώματα, νεοπλάσματα του προστάτη, καλώς διαφοροποιημένα νεοπλάσματα του μαστού, ορισμένοι τύποι λεμφωμάτων κ.λπ.

Για την καλύτερη ενημέρωσή σας συνοδεύουμε την επιστολή με δύο άρθρα ανασκόπησης, όπου μπορείτε να πληροφορηθείτε τις βασικές αρχές, τις εφαρμογές, τα πλεονεκτήματα και τα μειονεκτήματα της τεχνικής της ολόσωμης διάχυσης. Σε αυτά υπάρχουν βιβλιογραφικές αναφορές για μεγάλο αριθμό νεοπλασματικών νόσων και συγκριτικές μελέτες με το PET/CT.

Ταυτόχρονα είμαστε στην διάθεση σας για οιοσδήποτε πληροφορίες θελήσετε, όσον αφορά διαγνωστικά ή πρακτικά θέματα.

Με εκτίμηση

Ανδρέας Παπαδόπουλος

Διδάκτωρ του Πανεπιστημίου Αθηνών

Diffusion-Weighted MR Imaging for Whole Body Metastatic Disease and Lymphadenopathy

Russell N. Low, MD^{a,b,*}

KEYWORDS

- Fast imaging • Echo planar imaging
- Diffusion-weighted imaging • MR imaging
- Diffusion-weighted whole-body imaging with background body signal suppression
- Whole body imaging

Diffusion is a physical property that describes the microscopic random movement of molecules in response to thermal energy. Also known as Brownian motion, diffusion may be affected by the biophysical properties of tissues such as cell organization and density, microstructure and microcirculation. Diffusion weighted (DW) imaging uses pulse sequences and techniques that are sensitive to very small-scale motion of water protons at the microscopic level. Single shot echo planar imaging (EPI) DW imaging is used to provide very rapid imaging sensitive to subtle small-scale alternations in diffusion. Areas of restricted water diffusion are displayed as areas of high signal intensity.^{1–11}

The application of DW imaging for the evaluation of intracranial abnormalities, such as acute cerebral infarcts, is well established.¹⁰ DW imaging often shows areas of altered diffusion in the abnormal brain long before any changes are manifested on conventional anatomic MR images. However, the challenges posed by DW imaging of the abdomen and pelvis initially limited its application for body MR imaging. With use of DW imaging, artifacts related to physiologic motion, susceptibility, and chemical shift are compounded by inherent limitations in signal-to-noise ratio and image resolution. The larger fields of view used for abdominal imaging accentuate many of the artifacts inherent in DW imaging and single shot EPI.^{7,11}

Hardware and technical advances in MR imaging, including rapid echo planar imaging, larger amplitude gradient systems, multi channel coils, and parallel imaging techniques, have overcome many of these limitations and, as a result, DW imaging is feasible for abdominal and pelvic MR imaging. By allowing for more rapid imaging with shorter echo time, reduced echo train length, and more rapid k-space filling, many of the artifacts inherent to DW imaging can be reduced.^{7,11,12}

Oncologic applications of DW imaging take advantage of restricted diffusion shown by most tumors.^{4,7,9–11} The higher cellularity of solid tumors and their increase in cell membranes per unit volume results in restriction of water movement and corresponding high signal intensity on DW images (**Fig. 1**). Areas of tumor necrosis show a decrease in tumor cellularity with an associated increase in diffusion and loss of signal on DW images. Similarly, tumor edema or cystic components of a tumor will show an increase in water diffusion and loss of signal on DW images.⁷

The routine use of DW imaging for abdominal and pelvic oncologic MR imaging is being evaluated. Recent works have described the use of single shot EPI DW imaging for evaluation of lymphadenopathy,^{11,13} liver tumors (**Fig. 2**),^{14–23}

^a Sharp and Children's MRI Center, 7901 Frost Street, San Diego, CA 92123, USA

^b San Diego Imaging, Inc., 7901 Frost Street, San Diego, CA 92123, USA

* Sharp and Children's MRI Center, 7901 Frost Street, San Diego, CA 92123.

E-mail address: rlow52@yahoo.com

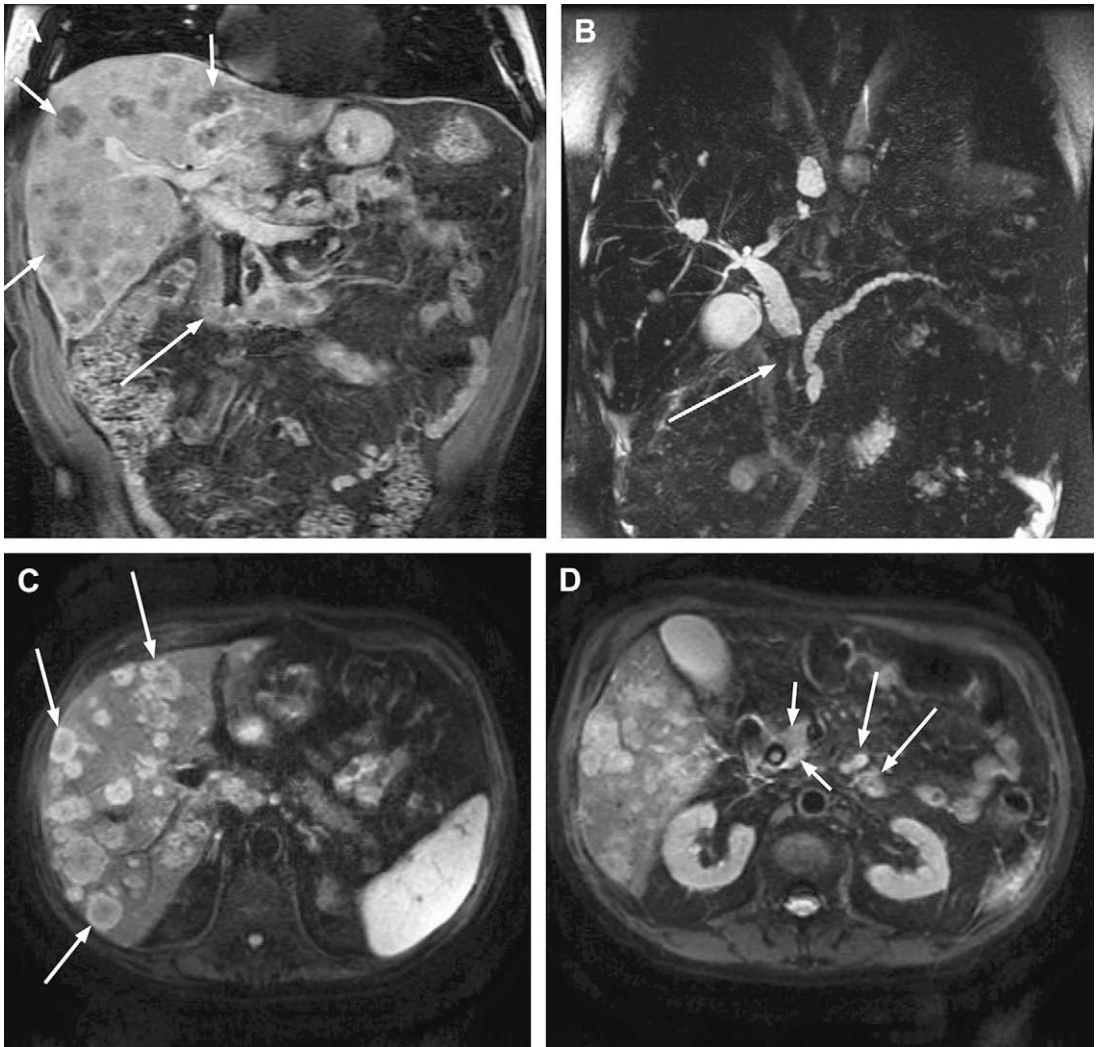


Fig. 1. 71-year-old man with pancreatic cancer. Coronal gadolinium-enhanced 3D FSPGR image (A) shows tumor (*long arrow*) encasing a biliary stent and liver metastases (*short arrows*). 3D MRCP (B) shows a double duct sign with obstruction of the common bile duct (*arrow*) and the pancreatic duct. Breath-hold DW image (C) b-value 400 s/mm^2 confirms multiple liver metastases (*arrows*) all showing restricted diffusion. Note the high contrast of the liver metastases and their sharp definition on this image obtained during suspended respiration. Breath-hold DW image (D) b-value 400 s/mm^2 at a lower level depicts tumor (*short arrows*) encasing the biliary stent and retroperitoneal nodal metastases (*long arrows*).

renal masses,^{24–30} prostate cancer,^{31,32} and colorectal cancer (see **Fig. 2**),^{33,34} pancreatic cancer,³⁵ uterine cancer,^{36–39} ovarian tumors,³⁹ peritoneal tumor,⁴⁰ and lung cancer.⁴¹ Prior studies have documented the value of DW imaging for tumor detection in the abdomen and pelvis when added to routine unenhanced and gadolinium-enhanced MR imaging in the oncology patient.⁴ The ability to generate qualitative and quantitative data using an entirely new contrast mechanism makes DW imaging an attractive tool for tumor assessment in the oncology patient.

TECHNICAL CONSIDERATIONS

Abdominal DW imaging can be performed on commercially available high field MR systems. Most vendors currently use a single shot spin-echo EPI pulse sequence for DW imaging. DW imaging can be performed as a breath-hold acquisition or as a breathing-averaged acquisition with multiple excitations.^{1–4} The later may be acquired as a free breathing or respiratory triggered acquisition.¹¹ In the DW pulse sequence, paired diffusion sensitizing gradients are centered on either side

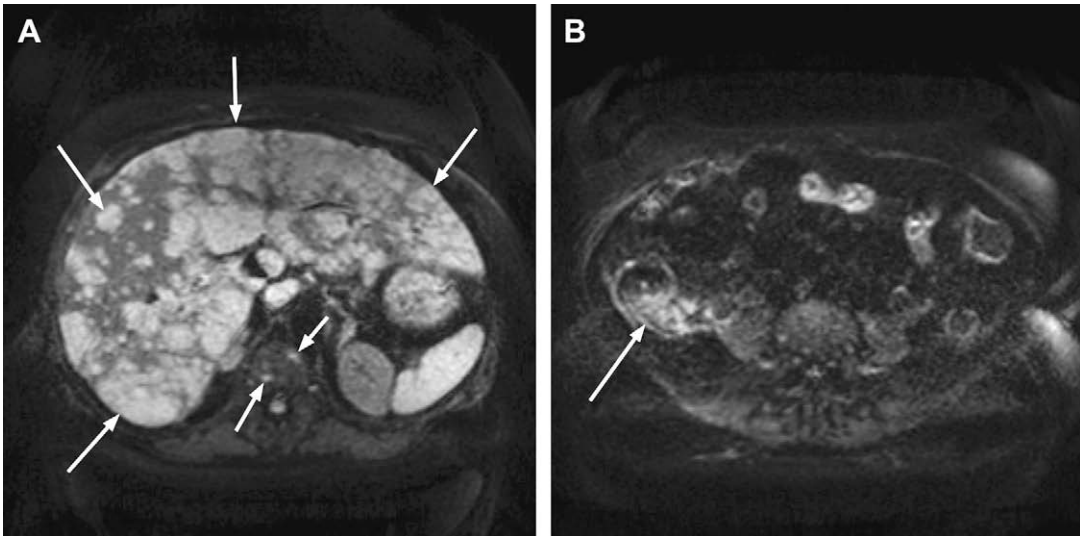


Fig. 2. 66-year-old man with colon cancer. Breath-hold DW image (A) b-value 400 s/mm² depicts innumerable liver metastases (*long arrows*) replacing most of the liver parenchyma. Osseous metastases (*short arrows*) are present in the thoracic spine vertebral bodies. Breath-hold DW image (B) b-value 400 s/mm² shows a mass in the right lower quadrant representing the patient's primary colon carcinoma.

of the 180 degree refocusing pulse. In the absence of motion, water molecules will acquire phase information from the first diffusion gradient that will be refocused by the second diffusion gradient with no net change in signal. However, with moving water molecules the situation is different. The water molecules will accumulate phase information from the first gradient that will not be completely refocused by the second diffusion gradient because of movement of the water molecule producing a loss of signal. The paired diffusion gradients will thus detect water motion as areas of signal loss.^{1,7} Tumors with a higher cellular density possess more cell membranes per unit volume, which restricts mobility of water molecules and diffusion. These tumors will exhibit restricted diffusion and corresponding high signal on DW imaging.

The sensitivity of the DW imaging sequence to water motion can be varied by changing the b-value, which depends on the amplitude and the timing of the paired bipolar diffusion sensitizing gradients.⁷ One typically acquires at least two b-values of 0 s/mm², combined with a second intermediate to a high b-value of 400–1000 s/mm². Acquiring additional b-values will improve the accuracy of the quantitative data obtained from DW imaging. Higher b-values result in more diffusion weighting with better background suppression, at the expense of reduced signal and increasing artifacts.^{7,11} At our institution, clinicians typically use b-value 0 s/mm² combined with intermediate b-values of 400–600 s/mm². For anatomic DW imaging, these intermediate

b-values achieve reasonable diffusion weighting while maintaining good image quality.

Diffusion experiments can be independently made in the phase, frequency, or slice directions by applying the diffusion gradient in the selected direction. One may also combine the diffusion signal from all three directions to create a summed image known as an index or magnitude diffusion image.⁷ A summed diffusion image loses its directional information but will improve scanning efficiency, allowing for shorter breath hold scan times while maintaining signal–noise-ratio.

Fat suppression is implemented to improve the contrast to background ratio on the DW images. Fat suppression can be accomplished with a short inversion time inversion recovery prepulse (STIR) sequence for maximal background suppression.^{7,11} This may be particularly advantageous for whole body diffusion where suppression of all background tissues is desirable when generating inverted maximum intensity projections (MIPs) of the DW dataset.¹¹ In our experience, for anatomic DW imaging, less complete suppression of background tissues is actually preferable to facilitate anatomic localization of tumors relative to adjacent anatomy. For anatomic DW imaging, fat suppression with spectral presaturation by inversion recovery (SPIR) prepulse or a frequency selective chemical shift selective (CHESS) prepulse achieves an optimal balance of partial background suppression to increase tumor conspicuity while maintaining anatomic landmarks for tumor localization.⁷

Phased array surface coils are used when performing anatomic DW imaging to improve signal-to-noise ratio and overall image quality. Surface coils also allow one to use parallel imaging, which reduces scan time. The read-out time is also decreased with SENSE, which reduces some of the artifacts that are inherent with DW imaging. Similarly, these artifacts may also be minimized by using a minimum echo time (TE) and decreasing the resolution in the frequency direction.^{7,11}

The following is a typical protocol for breath-hold abdominal DW imaging used for anatomic imaging.

- Single Shot Spin-Echo EPI
- Phased array surface coil
- B-value 0, 500 s/mm²
- Slice thickness 7 mm, 1 mm interslice gap
- FOV 320–400 cm
- TR 2700
- TE 58 (min)
- Matrix 115 x115
- SPIR fat suppression
- 24 slices
- 2–3 nex
- Direction of motion probing gradients: phase, frequency, slice
- Acceleration factor 2
- Time: 24 sec breath-hold

Whole-body DW imaging is performed with multiple stacks of axial DW acquisitions covering large anatomic areas that may include head, neck, chest, abdomen, pelvis and lower extremities.^{11,42–47} The axial plane is chosen to minimize image distortion. A three- to five-station whole-body DW imaging protocol can be prescribed with overlap between the stations. Some MR systems allow for whole-body imaging with multiple surface coils. On other systems, whole-body DW imaging will require imaging with the integrated large body coil. After the multiple axial DW imaging stacks are prescribed and pre-scanned, automatic table movement between stations facilitates scanning and data acquisition.

Post-processing the whole-body DW imaging typically includes binding the multiple stacks of axial DW images into one large data set. The large whole-body DW data set can be further post processed by generating a 3D model using a MIP post-processing algorithm. The MIP can be inverted to create an image in which tumors are displayed as dark structures on a white background. Automation of post processing of the whole-body DW imaging dataset is available from some vendors.

Typical imaging parameters for whole-body DW imaging include:

- Single shot spin-echo EPI
- Body coil

- B-value 600–1000 s/mm²
- 3 stations – axial
- 50 slices/station 6 mm thickness
- FOV 420 × 345
- TR 3560 TE 58 (min)
- Matrix 104 × 288 phase x frequency
- STIR fat suppression
- Covers 30 cm per stack
- NEX 4
- Direction of motion probing gradients: phase, frequency, slice
- Time: 1:39 per stack-free breathing

DIFFUSION-WEIGHTED IMAGE ANALYSIS AND DISPLAY

DW images can be evaluated qualitatively by observing changes in signal intensity from areas of the image with minimal restriction of water, such as liver parenchyma, to those with high restriction of water diffusion, such as tumors. In the author's experience, the DW images typically show excellent tumor conspicuity but relatively poor anatomic localization because of suppression of background tissues. For this reason, the DW images are often most useful when interpreted in conjunction with routine anatomic MR images. The DW images can be evaluated as a separate series side-by-side with the T1-, T2- and gadolinium-enhanced acquisitions. In the future, fusion of DW images with anatomic MR images may further improve image interpretation.

Simple visual inspection of magnitude DW images can lead to a potential pitfall and image misinterpretation because observed signal represents the combination of effects from water diffusion and T2 relaxation.^{7,11,46} Tissues with prolonged T2 relaxation may appear bright on a DW image representing "T2 shine through." This effect is decreased with higher b-values. With an intermediate b-value, T2-shine through typically occurs with fluid-containing structures, such as gastrointestinal tract, gallbladder, urinary, bladder, and cerebrospinal fluid. Cystic lesions in the liver, kidney, and elsewhere may show similar high signal on DW images because of their prolonged T2 relaxation. Most of these fluid filled structures will show at least partial suppression on DW images obtained with an intermediate b-value. In practice, it is fairly simple to distinguish high signal on a DW image that is caused by T2 shine through from tumors with restricted diffusion. Tsushima and colleagues⁸ confirmed the importance of comparing high b-value DW images with T2-weighted images or fused images for maximal accuracy in malignant tumor screening. By comparing the DW images with T2-weighted

images or the B0 DW images, one can identify structures that are fluid-containing on the T2-weighted images or B0 images. A more rigorous elimination of high signal from T2 prolongation can be achieved using apparent diffusion coefficient (ADC) maps, which depict changes in signal intensity that are solely caused by water diffusion. On the ADC map, a tumor with restricted diffusion is displayed as an area with low signal intensity as opposed to the DW image in which the tumor is of high signal intensity.^{7,42}

A qualitative display of DW images can also be performed following simple post-processing of the data set to generate thin section MIPs reformatted into the coronal or sagittal planes. A whole-volume MIP can also be generated creating a 3D model that can be rotated to display anatomic relationships of tumor to normal structures. This volumetric approach to displaying the DW imaging data requires maximal background suppression (see DWIBS below) and in our experience works best for lymphadenopathy.

Quantitative analysis of DW images can be performed if at least two b-values are obtained.^{15,16,30,48-51} Obtaining additional b-values will increase the accuracy of measurements. This quantitative analysis can be performed easily on the MR scanner or workstation, generating ADC parametric maps that are independent of field strength and T2-shine through. By drawing regions of interest on the ADC map over tissues of interest, a numerical value known as the ADC is generated.⁷ The ADC value can help to characterize tumors as benign or malignant and can assess interval change in a tumor in response to therapy. Areas of highly cellular tumor with restricted

diffusion demonstrate low ADC values while tissues with free water diffusion demonstrate high ADC values. It has also been observed quantitatively that, following therapy, tumors show a significant increase in ADC values with a corresponding loss of signal on visual inspection of the DW image.^{21,50-53}

TUMOR DETECTION

The addition of DW imaging to conventional abdominal and pelvic MR imaging improves the detection of many types of primary and metastatic tumor in oncology patients (Fig. 3).⁴ This improved sensitivity for tumor is caused by the improved conspicuity of tumor on DW imaging compared with conventional T1-, T2-, and gadolinium-enhanced imaging. On DW imaging, background tissues are relatively suppressed while most forms of tumor show restricted water diffusion, which results in moderate to marked tumor conspicuity.

In a study of 169 oncology patients, the addition of breath-hold DW imaging to routine abdominal MR images resulted in detecting additional sites of tumor in 40% and 46% of patients for two observers⁴ when compared with conventional MR imaging alone. An intermediate b-value 500 s/mm² was used. The additional sites of tumor detected on the DW imaging include 43 patients with lymphadenopathy, 15 with peritoneal metastases, 1 with a renal tumor, 12 with liver tumors, and 2 with osseous tumors. For observer two, the corresponding sites of addition tumor on DW images included 37 with lymphadenopathy, 12 with peritoneal tumors, 1 with renal tumors, 6 with liver tumor, 4 with osseous tumor, and 1 with a gastrointestinal

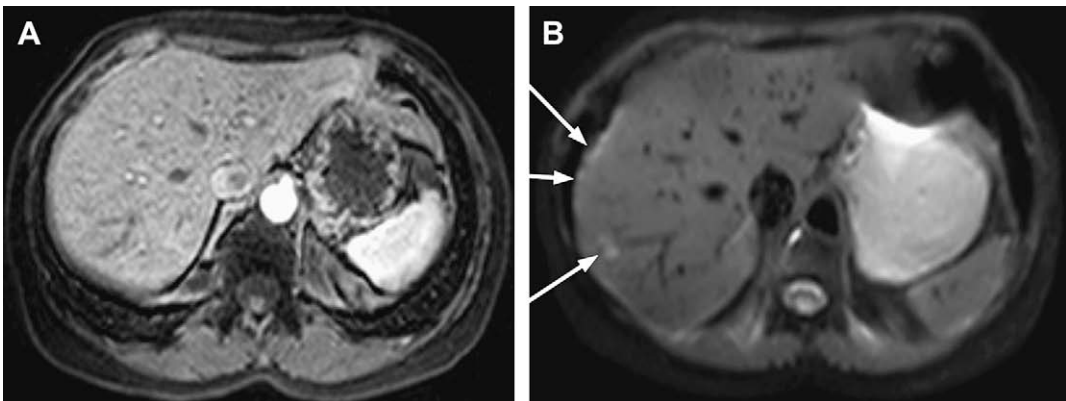


Fig. 3. 60-year-old woman with breast cancer. Arterial phase gadolinium-enhanced 3D FSPGR image (A) is unremarkable without evidence of liver metastasis. T1-weighted, T2-weighted, and portal venous phase gadolinium-enhanced images (not shown) were also normal. Breath-hold DW image (B) b-value 20 s/mm² shows small subcapsular and parenchymal liver metastases (arrows). Findings were confirmed by biopsy. This case demonstrates the sensitivity of DW imaging to small tumors. The "black blood" appearance of the DW image facilitates depiction of small perivascular tumors.

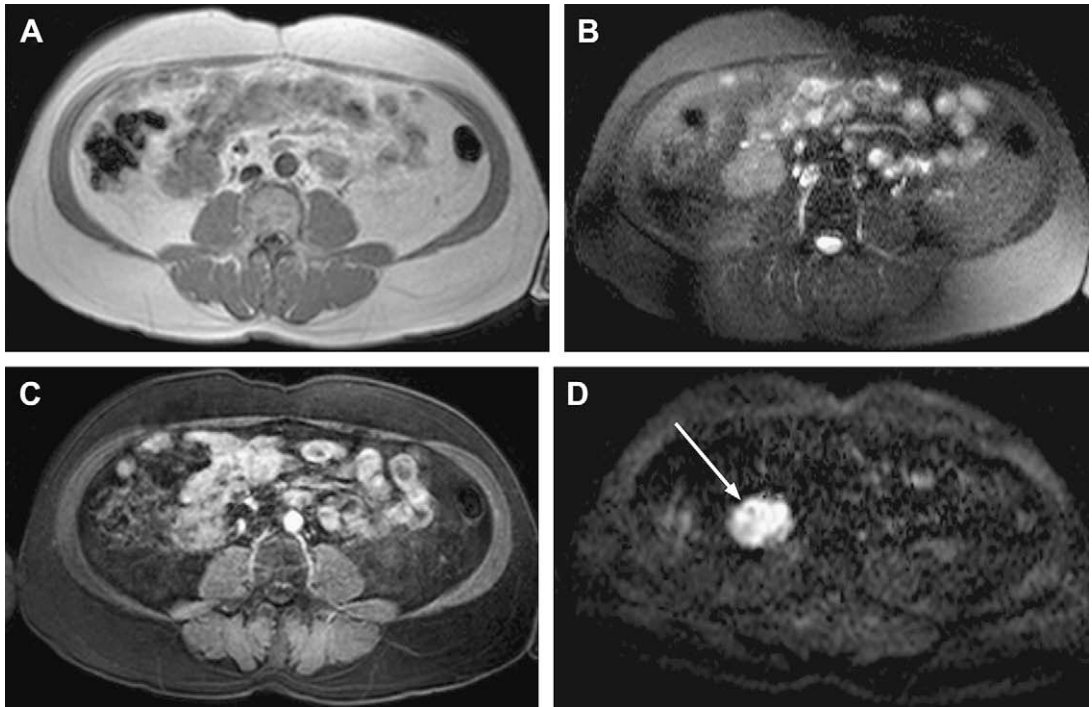


Fig. 4. 68-year-old man with prostate cancer and rising PSA. T1-weighted (A), T2-weighted (B), and fat suppressed gadolinium-enhanced SGE (C) images were interpreted as showing unopacified bowel but no evidence of tumor. Breath hold DWI (D) b-value 500 s/mm² shows a 3 cm right-sided retroperitoneal tumor (arrow).

tumor. The conventional MR examination was entirely normal while the DW images showed tumor in 6%–7% of patients (Fig 4).

Studies evaluating DW imaging for depicting liver metastases have found similar improvements in lesion detection compared with conventional unenhanced and contrast enhanced MR imaging (Fig. 5). Parikh and colleagues²³ compared DW imaging and breath-hold T2-weighted images for detection and characterization of liver metastases. Overall detection was significantly higher for DW imaging (87.7%) versus T2-weighted (70.1%) imaging, while lesion characterization was not significantly different. Nasu and colleagues²² found that the addition of DW imaging to T1-weighted and T2-weighted MR imaging showed higher accuracy in the detection of hepatic metastases than did reading of SPIO-enhanced MR images. In a comparison, DW imaging performed before and after SPIO administration found a synergistic effect between iron oxides and DW imaging noting that post-SPIO DW imaging showed improved contrast-to-noise ratio between malignant lesions and liver.⁵⁴

DW imaging can be useful to depict tumors in the nonsolid abdominal organs, such as the gastrointestinal tract and peritoneum (Figs. 6

and 7).^{33,34,40} In evaluating patients with colorectal cancer, Nasu and colleagues³³ noted that tumors were hyperintense on DW images using a b-value 1000 s/mm² and were easily distinguished from the normal colon wall and feces, which was always hypointense. Primary and metastatic tumor in the chest, involving the lung parenchyma, mediastinum, pleura, and chest wall, are also well depicted on DW imaging (Fig. 8).⁴¹

DW imaging improves the depiction of a wide spectrum of primary and metastatic tumors in the abdomen and pelvis. When implemented as a breath-hold acquisition the DW imaging will add very little time to the examination and can be routinely performed in all patients.^{4,7,11,42} It is important to note that areas of restricted diffusion on DW images are not specific for tumor. Normal lymph nodes show restricted diffusion and are displayed as hyperintense on DW images.^{7,11,42} Similarly, infectious and inflammatory conditions will show restricted diffusion. For example, pancreatitis, cholecystitis, osteomyelitis, an abdominal abscess, and colitis will show restricted diffusion on DW imaging.^{55–58} Therefore, interpretation of DW images requires consideration of the patient's clinical presentation and history, as well as an assessment of conventional MR images.

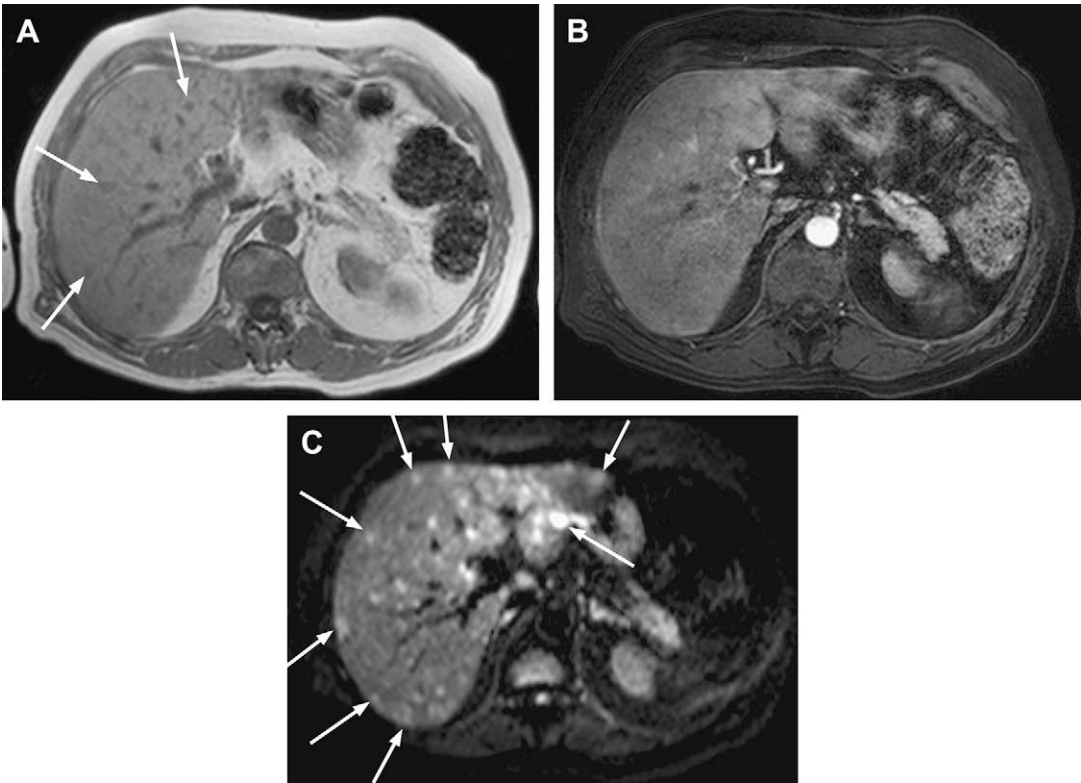


Fig. 5. 56-year-old man with prostate cancer. T1-weighted image (A) shows a few scattered small liver lesions (arrows). Arterial phase gadolinium-enhanced 3D FSPGR image (B) is unremarkable, as were the portal venous phase and equilibrium phase images (not shown). Breath-hold DW image (C) b-value 500 s/mm² depicts many additional small liver metastases (arrows).

WHOLE-BODY DIFFUSION-WEIGHTED IMAGING

Diffusion-weighted whole-body imaging with background body signal suppression (DWIBS) was first

described by Takahara and colleagues¹¹ in 2004 (Fig. 9). Using DW imaging with a short TI inversion recovery-echo planar imaging (STIR-EPI) sequence and free breathing scanning, the author generated

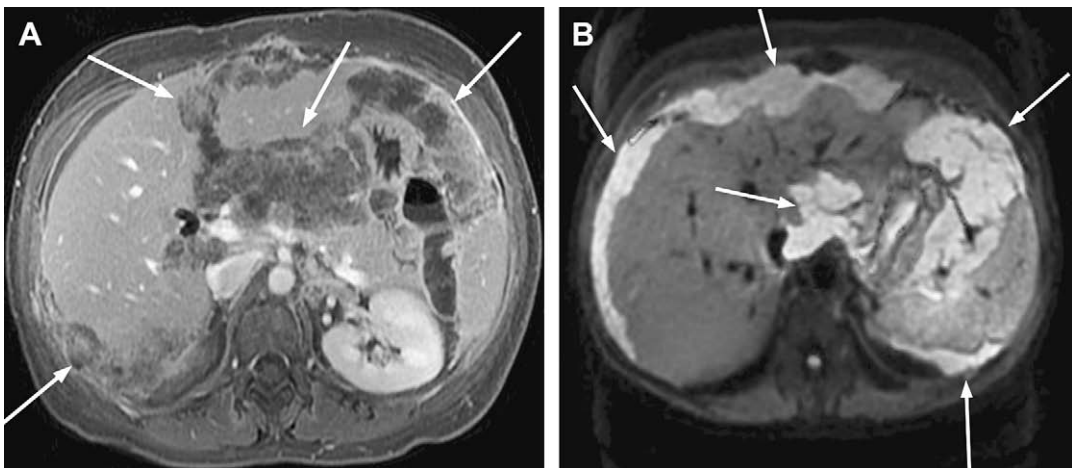


Fig. 6. Patient with pseudomyxoma peritonei. Delayed gadolinium enhanced SGE MR image (A) depicts bulky upper abdominal peritoneal tumors (arrows) encasing the liver, spleen, stomach, and pancreas. Breath hold DW image (B) b value 400 s/mm² depicts bulky upper abdominal peritoneal tumors (arrows) showing restricted diffusion. Ascites is low signal intensity on DW images while tumors are high signal intensity.

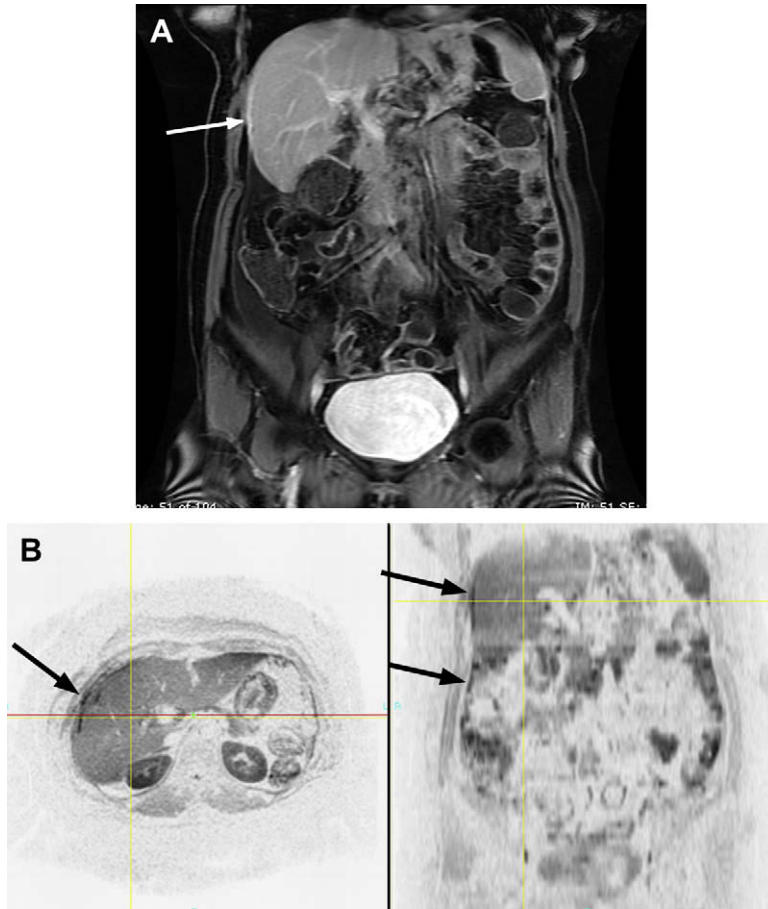


Fig. 7. Patient with treated ovarian cancer and rising serum CA-125 value. Coronal gadolinium enhanced 3D FSPGR image (A) depicts a thin rim of right subphrenic peritoneal tumor (*arrow*). Reformatted thin section axial and coronal DW images (B) b-value 400 s/mm² confirm a thin rim or right subphrenic peritoneal tumor adjacent to the right hepatic lobe. Thin section reformatted images are useful for anatomic localization of tumors in multiple planes.

whole-body DW images that depicted various tumors and lymphadenopathy, providing volumetric diffusion weighted images of the entire body. These projectional volumetric images provide a quick display of tumor in the chest, abdomen, and pelvis and can simplify display of complex cases facilitating comparison with follow-up MR examinations (**Fig. 10**).

Interpretation of DWIBS examinations should be performed by reviewing the source images (see **Fig. 8**). Projectional MIP images can be useful for displaying tumor relationships but can also mask a tumor or falsely create a pseudotumor.^{11,42-47} The potential for false positive interpretations with whole-body diffusion may be because of incomplete background suppression, T2 shine-through, and susceptibility artifact. Because of the degree of background suppression, the DWIBS images often lack information for anatomic localization. For this reason, viewing the DWIBS images

side-by-side with anatomic MR images is essential for accurate interpretation (**Fig. 11**). Fusion of the DW images and anatomic images may provide the most accurate means of image display.

Certainly, not all structures showing restricted diffusion on a whole-body DW imaging study are tumor. Some normal anatomic structures may show restricted diffusion and be displayed as hyperintense on DWIBS images. For example, normal lymph nodes are readily apparent on whole body DW images and probably cannot be distinguished from malignant nodes based solely upon their appearance on DW imaging.^{7,42} Other normal structures including brain, salivary glands, tonsils, spleen, gallbladder, small intestine, colon, prostate, testes, endometrium, cerebrospinal fluid, and bladder may exhibit high signal intensity on DWIBS images.⁴² Finally, just as with anatomic DW imaging, restricted diffusion can be seen in benign inflammatory and infectious diseases.⁵⁵⁻⁵⁸

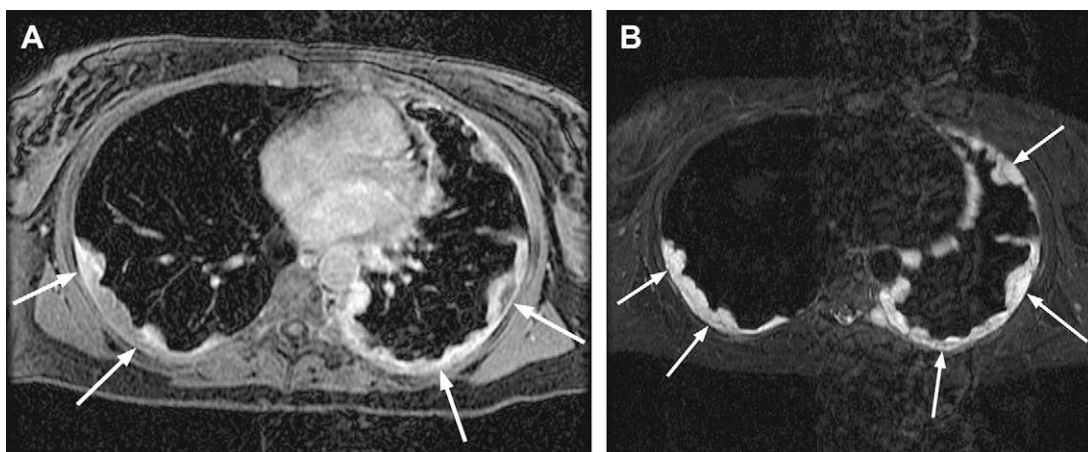


Fig. 8. Patient with appendiceal cancer. Gadolinium-enhanced SGE image (A) through the chest demonstrates bilateral enhancing pleural metastases (arrows). Breath hold DW image (B) b-value 500 s/mm^2 shows the bilateral pleural tumors. The marked tumor conspicuity facilitates depiction of the full extent of the pleural metastases.

Potential clinical applications for whole-body diffusion include staging of cancer because both the primary tumor and distant metastases demonstrate restricted diffusion.^{7,42} Small metastases can be easily seen because of suppression of background tissues. Certain anatomic areas, including the diaphragms and heart, may be problematic because of artifacts from susceptibility or motion. Interpretation of whole-body DW images in conjunction with anatomic MR imaging will increase overall accuracy for tumor depiction and staging.⁴²

Whole-body diffusion can also be used to evaluate response of primary tumor and metastases to interval chemotherapy or radiation therapy.⁴² After the tumors are depicted, follow-up whole body diffusion can be used to monitor changes in tumor size and ADC values with treatment. Distinguishing residual or recurrent tumor from post-treatment benign changes may be a role for DW imaging but will need to be validated with large patient groups.

One of the most compelling applications of whole-body DW imaging is the evaluation of lymphadenopathy in patients with predominantly nodal metastases.¹¹ Patients with lymphoma or leukemia are excellent candidates for surveillance with whole body DW imaging (Figs. 9 and 10). Because of suppression of background tissues, the highly cellular lymph nodes are depicted with very high tumor-to-background tissue contrast. Even small nodes are easily depicted. In addition, the volumetric display of the whole-body DW dataset can give a more accurate presentation of the location and distribution of nodal tumor than can routine planar anatomic MR images. Follow-up whole-body DW imaging very quickly displays any interval

change in nodal status. Interpretation of whole-body DW examination for lymphadenopathy is simplified by the predictable locations of lymph nodes in the neck, chest, abdomen, and pelvis. In contrast, the volumetric display of other disseminated tumors involving the peritoneum, bowel, and mesentery can be confusing. In the later situation, thin section multiplanar reformatted images or subvolume MIPs may be a more effective way to display data from whole-body DW imaging.

Comparisons of whole-body DW imaging and PET have been favorable. Ohno and colleagues⁴³ found that in patients with non-small cell lung cancer (NSCLC), whole-body MR imaging with DW imaging can be used for M-stage assessment with accuracy as good as that of PET/CT. In a comparison of DWIBS and FDG PET, Komori and colleagues⁴⁵ found 25 (92.6%) of the 27 malignant lesions were detected visually with DWIBS imaging in contrast to 22 malignant tumors (81.5%) with ^{18}F -FDG PET/CT imaging. Compared to PET/CT, whole-body DW imaging offers several important advantages, including lack of ionizing radiation and much shorter examination times. Currently, the effective radiation dose per PET/CT examination is about 25 mSv and the examinations require 2–3 hours to complete. Whole-body DW imaging can be performed safely without radiation exposure in a fraction of the time required for PET/CT.

Application of the whole-body DW technique for specific malignancies has also been evaluated. For colorectal cancers, Ichikawa and colleagues³⁴ evaluated the usefulness of DWIBS. Visual assessment of the DWIBS images resulted in high sensitivity (91%, 20/22) and specificity (100%, 15/15) for detection of the primary tumor.

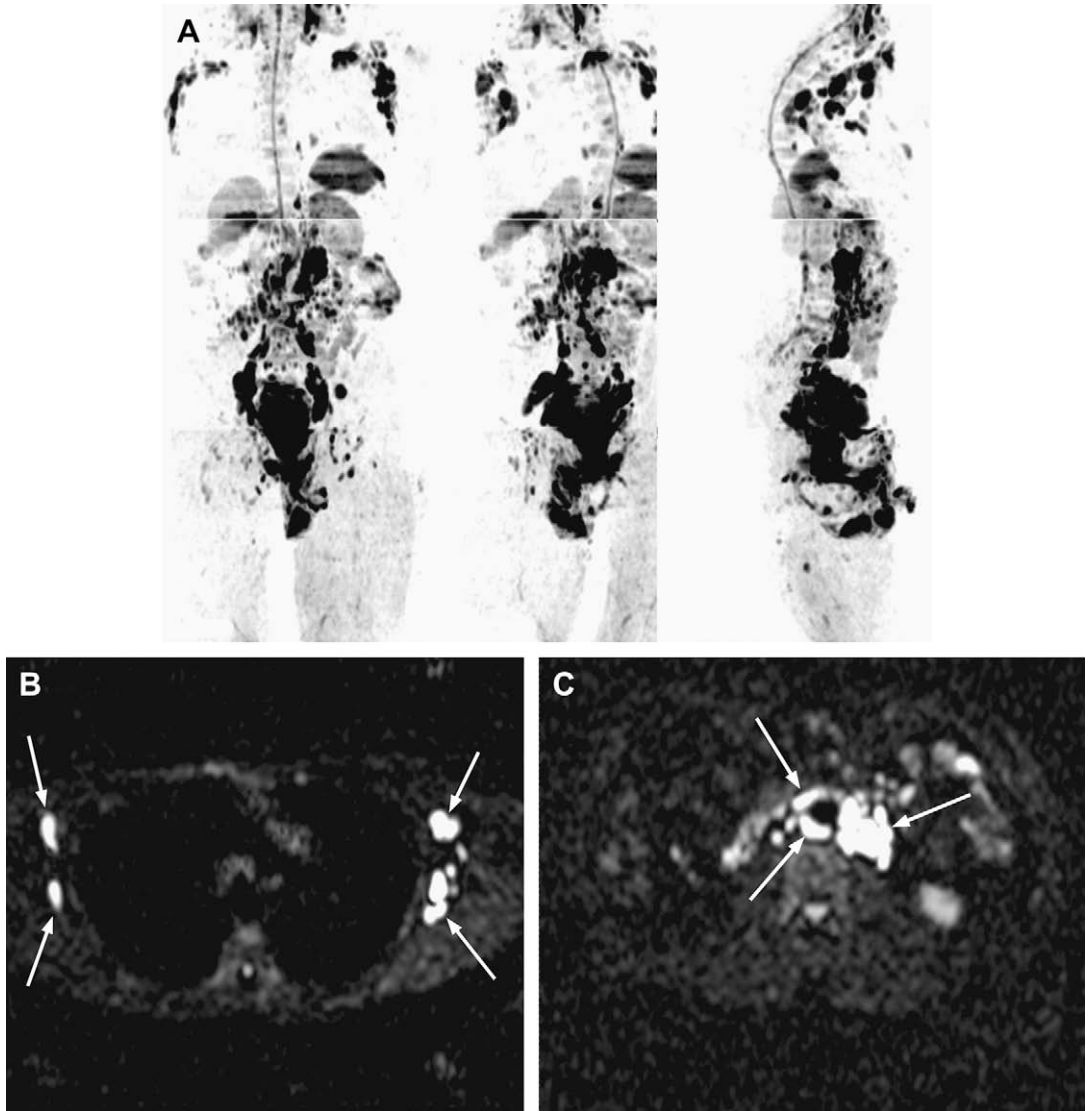


Fig. 9. 82-year-old man with lymphoma. Three projections (A) from the inverted MIP of a whole-body DW imaging examination show bulky lymphadenopathy in the neck, chest, abdomen and pelvis. Source DW image (B) b-value 500 s/mm² obtained through the chest shows bilateral axillary lymph nodes (arrows). Note the marked high contrast of the lymph nodes. DW image (C) b-value 500 s/mm² obtained through the abdomen depicts moderately bulky retroperitoneal lymphadenopathy (arrows).

For pancreatic adenocarcinoma, 26 patients with pathologically proven pancreatic adenocarcinoma and another 23 controls, assessment of the DWBS images resulted in high sensitivity (96.2%, 75/78) and specificity (98.6%, 68/69).³⁵

DEPICTION OF RECURRENT TUMOR

Detecting recurrent tumor is an imaging challenge that demands high levels of sensitivity and specificity. Small-volume tumor recurrence must be accurately distinguished from normal anatomy

as well as from benign sequela of therapy, including surgery, radiation, percutaneous ablation, and chemoembolization (Fig. 12). DW imaging provides such a high tumor-background contrast that its sensitivity for small tumors is markedly increased over normal anatomic MR imaging (Figs. 13 and 14). In the author's experience, DW images may depict small volume tumor recurrence before other conventional anatomic images are abnormal.⁴ The specificity of areas of restricted diffusion on DW imaging is still being evaluated. It is possible that a quantitative analysis

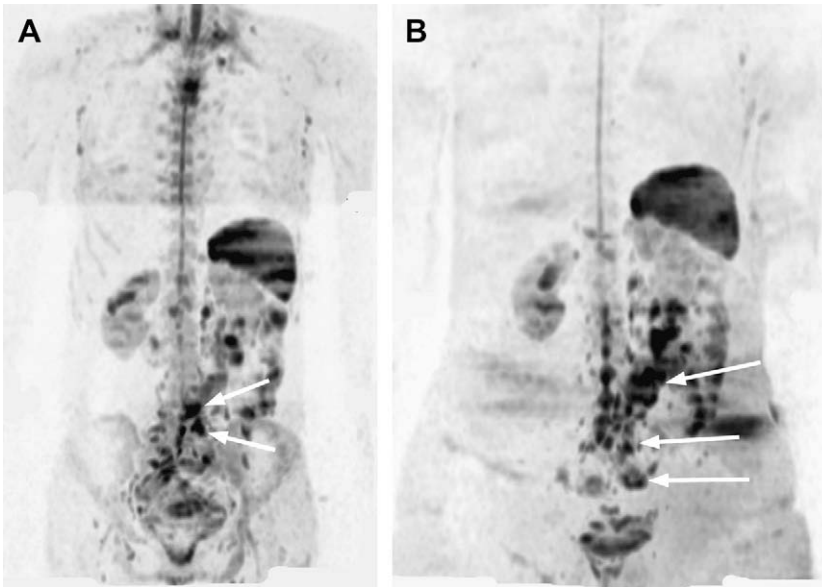


Fig. 10. 55-year-old man with lymphoma. Whole-body DW imaging examination performed in December 2007 (A) shows small retroperitoneal lymph nodes (arrows). Follow-up whole-body DW imaging examination from July 2008 (B) shows interval progression of lymphadenopathy (arrows).

of DW imaging with ADC values will improve the distinction of small tumors from post therapeutic changes. For neuroimaging, distinguishing recurrent neoplasm from radiation necrosis can be challenging. Using DW imaging, significant differences have been found in maximal ADC values between radiation necrosis and recurrent tumor.⁵⁹

TUMOR CHARACTERIZATION

A quantitative analysis of DW images may allow one to distinguish benign from malignant tumors in the abdomen and pelvis. As a general rule, benign processes would be expected to have a higher ADC than highly cellular malignant

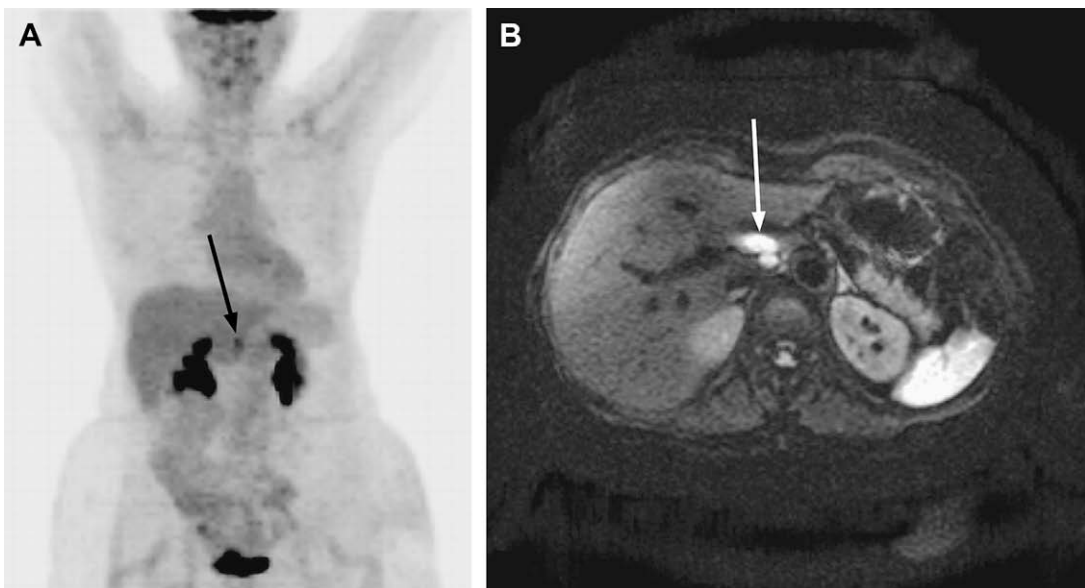


Fig. 11. 55-year-old woman with treated ovarian cancer and a rising serum CA-125 value. Inverted MIP from a whole-body DW imaging acquisition (A) shows a small focal lesion in the upper abdomen. Breath-hold DW image (B) b-value 400 s/mm² shows portal caval lymphadenopathy (arrow) representing nodal metastases.

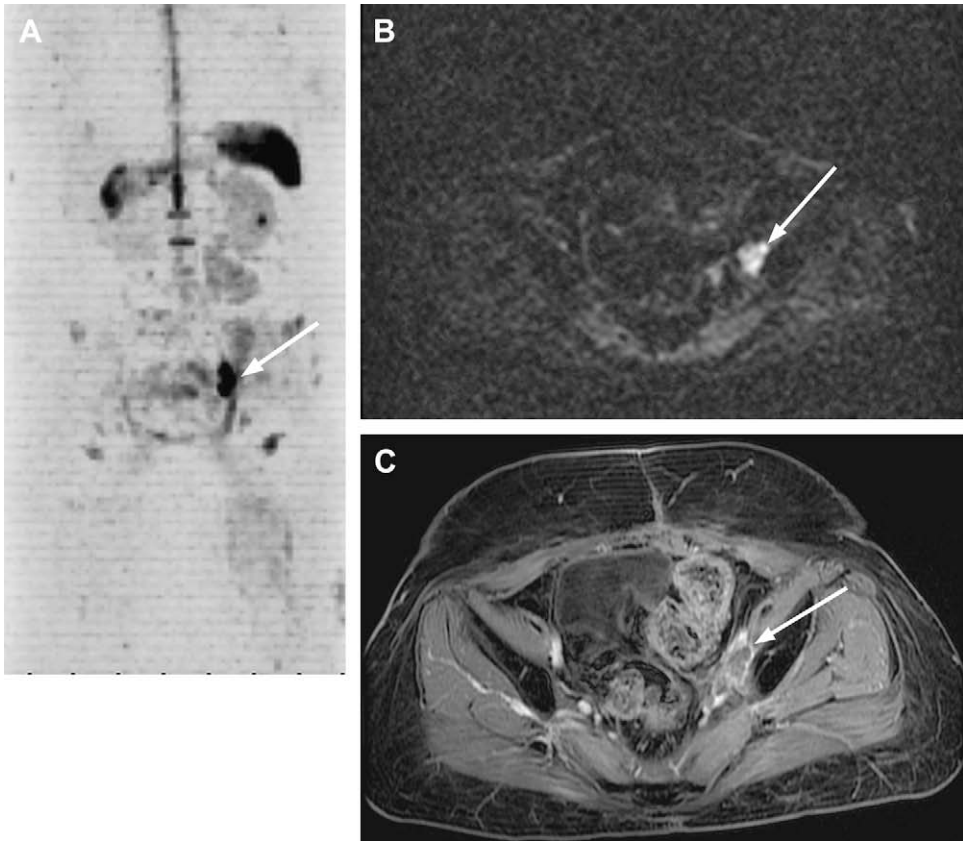


Fig. 12. 65-year-old man with colon cancer. Inverted MIP (A) from a whole-body DW imaging examination shows a focal intense area of restricted diffusion in the left pelvic sidewall. DW image (B) b-value 600 s/mm^2 shows a focal tumor in the left side of the pelvis. Fat suppressed, gadolinium-enhanced image (C) confirms the 2 cm left iliac nodal metastases (arrow).

process, which demonstrates restricted diffusion and lower ADC values. Some of the challenges in implementing this type of analysis include: variations in the ways that DW imaging is implemented on different scanners and obvious differences in DW imaging protocols, all of which will affect the numerical ADC value. It is also not surprising that there is considerable overlap in the ADC values for benign and malignant diseases. However, the ADC values obtained from DW imaging provide an intriguing new tool to characterize abdominal tumors.

In several studies, malignant liver tumors have shown significantly lower ADC values than benign liver cysts and hemangiomas.^{15,16} Renal masses may be similarly characterized with quantitative DW imaging. Zhang and colleagues⁴⁸ noted that renal tumors had significantly lower ADCs compared with benign cysts and that solid enhancing tumors had significantly lower ADCs compared with nonenhancing necrotic or cystic regions. Cystic renal neoplasms behave

differently than solid renal cell cancers on DW imaging. In one study, ADC values of cystic renal cell carcinomas were higher than those of clear cell carcinomas. The ADC value of cystic renal cell carcinomas overlapped with that of normal renal parenchyma but was less than that of a simple renal cyst.³⁰

ASSESSMENT OF RESPONSE TO THERAPY

This quantitative approach to diffusion imaging can also be used to assess tumor response to treatment.^{21,49–53} Initially, high-signal tumors with a low ADC have been observed to lose signal intensity with a corresponding increase in diffusion coefficient following treatment (Fig. 15). Hepatocellular cancer showed an increase in tumor ADC values following transcatheter chemoembolization.⁵⁰ Similarly, a significant increase in mean ADC value was observed in liver metastatic lesions that responded to chemotherapy (Fig. 16).²⁰

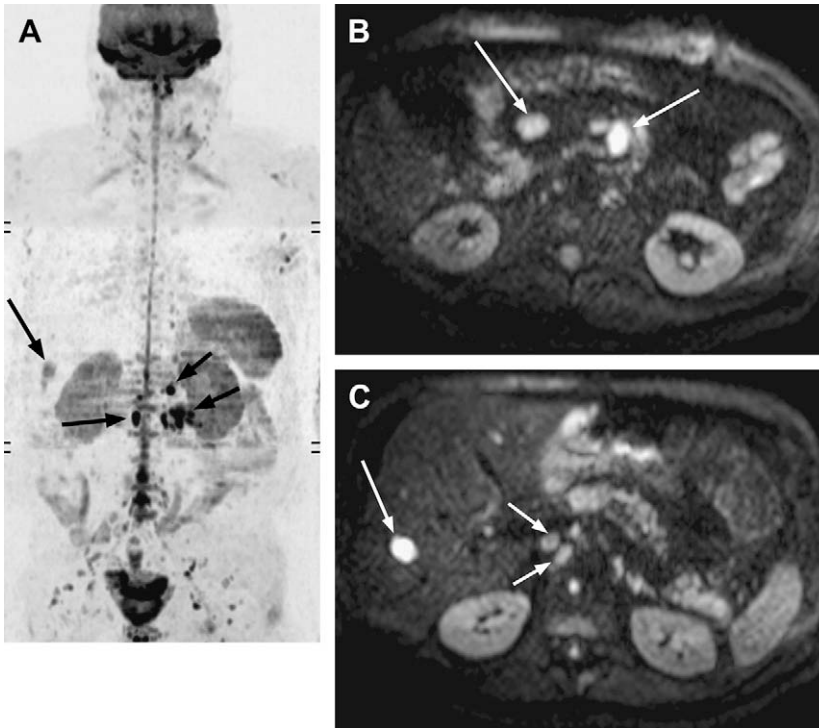


Fig. 13. 59-year-old man with pancreatic cancer status post Whipple procedure. Whole-body DW image (A) shows liver metastasis (*long arrow*) and retroperitoneal nodal metastases (*short arrows*). DW image (B) b-value 500 s/mm^2 confirms the moderately bulky retroperitoneal lymphadenopathy (*arrows*). DW image (C) b-value 500 s/mm^2 depicts liver metastasis (*long arrow*) and smaller retroperitoneal lymph nodes (*short arrows*). Findings represent recurrent pancreatic cancer.

PREDICTING RESPONSE TO THERAPY

Evaluating pretreatment ADC values of tumors may also shed light upon which tumors will respond to subsequent therapy. Koh and colleagues²⁰ noted that for colorectal hepatic metastases, high pretreatment mean ADC values

were predictive of poor response to chemotherapy. Similarly, Cui and colleagues⁵¹ evaluated patients with 38 responding and 49 nonresponding metastatic liver lesions from colorectal and gastric cancer. Pretherapy mean ADC values in responding lesions were significantly lower than those of nonresponding lesions ($P = .003$).⁵¹ DW

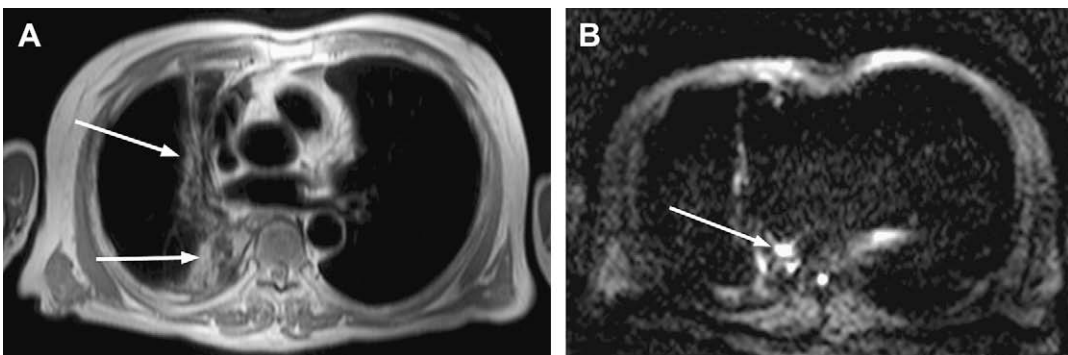


Fig. 14. Patient with lung cancer status post radiation therapy. T1-weighted image (A) show parenchymal changes from radiation therapy but no definite evidence of residual tumor. Breath hold DW image (B) b-value 500 s/mm^2 shows a small focal nodule with marked restriction of water diffusion. Findings represent tumor recurrence and correlated with results of subsequent PET scan (not shown).

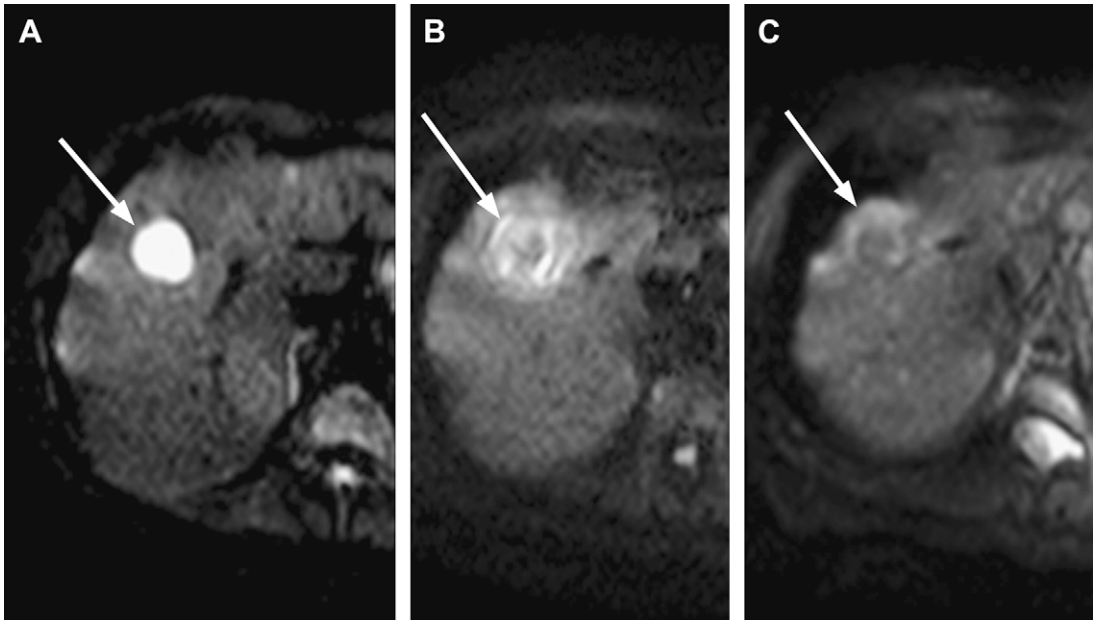


Fig. 15. Patient with a 2.5 cm hepatocellular cancer treated with radiofrequency ablation (RFA) shown on serial MR examinations. Pretreatment DW image (A) shows the focal HCC (*arrow*) with marked high signal intensity. Follow up DW image (B) obtained 3 months following treatment shows decrease in signal intensity of the treated HCC (*arrow*). Final DW image (C) obtained 8 months following treatment shows further loss of signal within the HCC indicating response to RFA. Corresponding increase in ADC value also indicates treatment response.

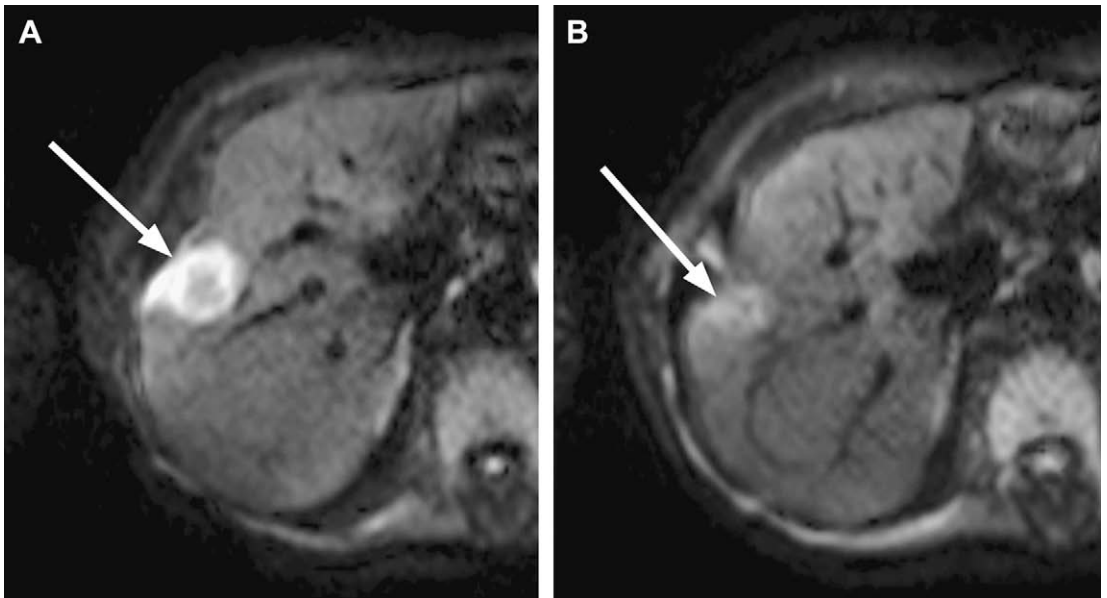


Fig. 16. Patient with metastatic colon cancer. Pretreatment DW image b-value 400 s/mm² (A) shows a 2.5 cm metastasis (*arrow*) in the right hepatic lobe with marked restriction of diffusion. Follow-up DW image b-value 400 s/mm² (B) obtained following chemotherapy shows decrease size of the metastasis and corresponding loss of signal intensity. Corresponding ADC values for the liver metastasis showed interval increase with treatment indicating response to chemotherapy.

imaging has been advocated as a means to assess tumor necrosis in patients with hepatocellular cancer undergoing chemoembolization⁵² with a linear correlation between ADC values and the degree of tumor necrosis at histopathologic evaluation.

SUMMARY

DW imaging provides qualitative and quantitative information that can be critical in the oncology patient. Accurate depiction of the primary tumor and whole-body metastases makes it an ideal sequence for oncologic imaging. Additional information obtained from a quantitative analysis of ADC values can be used to characterize tumors and assess response to treatment. Speculating on the future role of diffusion weighted body imaging compared with PET/CT is intriguing. DW imaging is clearly a powerful new tool that improves the sensitivity and specificity of body MR imaging for oncologic imaging. Because DW imaging does not provide true metabolic information, it seems unlikely to entirely replace PET/CT. Rather these two examinations will play complementary roles. There is growing concern about the radiation exposure and the cost of PET/CT. MR imaging combined with DW imaging is in a unique position to augment the role of PET/CT in cancer imaging. Initial evaluation with PET/CT might be used to identify sites of primary and metastatic tumor. Follow up MR imaging and DW imaging could be performed to monitor the tumor response to therapy. In other clinical settings, the limitations of PET/CT in depicting some tumors, including peritoneal metastases and small liver metastases, makes MR imaging with DW imaging the initial examination of choice. In the author's experience, DW imaging combined with conventional MR imaging leads to more accurate imaging diagnoses, better treatment decisions, and improved patient care.

REFERENCES

1. Ichikawa T, Haradome HH, Hachiya J, et al. Diffusion-weighted MR imaging with single-shot echo-planar imaging in the upper abdomen: preliminary clinical experience in 61 patients. *Abdom Imaging* 1999;24:456–61.
2. Yamashita Y, Tang Y, Takahashi M. Ultrafast MR imaging of the abdomen: echo planar imaging and diffusion-weighted imaging. *J Magn Reson Imaging* 1998;8:367–74.
3. Chow LC, Bammer R, Moseley ME, et al. Single breath-hold diffusion-weighted imaging of the abdomen. *J Magn Reson Imaging* 2003;18:377–82.
4. Low RN, Gurney J. Diffusion-weighted MRI (DWI) in the oncology patient: value of breath hold DWI compared to unenhanced and gadolinium-enhanced MRI. *J Magn Reson Imaging* 2007;25:848–58.
5. Bammer R, Auer M, Kelling SL, et al. Diffusion tensor imaging using single-shot SENSE-EPI. *Magn Reson Med* 2002;48:128–36.
6. Murtz P, Flacke S, Traver F, et al. Abdomen: diffusion-weighted MR imaging with pulse-triggered single-shot sequences. *Radiology* 2002;224:258–64.
7. Koh DM, Collins DJ. Diffusion-weighted MRI in the body: applications and challenges in oncology. *AJR Am J Roentgenol* 2007;188:1622–35.
8. Tsushima Y, Takano A, Taketomi-Takahashi A, Endo K. Body diffusion-weighted MR imaging using high b-value for malignant tumor screening: usefulness and necessity of referring to T2-weighted images and creating fusion images. *Acad Radiol* 2007;14:643–50.
9. Toney HC, De Keyser F. Extracranial applications of diffusion weighted magnetic resonance imaging. *Eur Radiol* 2007;17:1385–93.
10. Provenzale JM, Mukundan S, Barboriak DP. Diffusion weighted and perfusion MR imaging for brain tumor characterization and assessment of treatment response. *Radiology* 2006;239:632–49.
11. Takahara T, Imai Y, Yamashita T, et al. Diffusion weighted whole body imaging with background body signal suppression (DWIBS): technical improvement using free breathing, STIR and high resolution 3D display. *Radiat Med* 2004;22:275–82.
12. Bammer R, Keeling RL, Augustin M, et al. Improved diffusion-weighted single-shot echo-planar imaging (EPI) in stroke using sensitivity encoding (SENSE). *Magn Reson Med* 2001;46:548–54.
13. Sumia M, Sakihama N, Sumia T, et al. Discrimination of metastatic cervical lymph nodes with diffusion-weighted MR imaging in patients with head and neck cancer. *AJNR Am J Neuroradiol* 2003;24:1627–34.
14. Kim T, Murakami T, Takahashi S, et al. Diffusion-weighted single-shot echoplanar MR imaging for liver disease. *AJR Am J Roentgenol* 1999;173:393–8.
15. Taouli B, Vilgrain V, Dumont E, et al. Evaluation of liver diffusion isotropy and characterization of focal hepatic lesions with two single-shot echo-planar MR imaging sequences: prospective study in 66 patients. *Radiology* 2003;226:71–8.
16. Nakimoto T, Yamashita Y, Sumi S, et al. Focal liver masses: characterization with diffusion-weighted echo-planar MR imaging. *Radiology* 1997;204:739–44.
17. Taouli B, Martin AJ, Qayyum A, et al. Parallel imaging and diffusion tensor imaging for diffusion-weighted MRI of the liver: preliminary experience in healthy volunteers. *Am J Roentgenol* 2004;183:677–80.
18. Gourtsoyianni S, Papanikolaou N, Yarmenitis S, et al. Respiratory gated diffusion-weighted imaging of the

- liver: value of apparent diffusion coefficient measurements in the differentiation between most commonly encountered benign and malignant focal liver lesions. *Eur Radiol* 2008;18:486–92.
19. Bruegel M, Holzapfel K, Gaa J, et al. Characterization of focal liver lesions by ADC measurements using a respiratory triggered diffusion-weighted single-shot echo-planar MR imaging technique. *Eur Radiol* 2008;18:477–85.
 20. Koh DM, Scurr E, Collins D, et al. Predicting response of colorectal hepatic metastasis: value of pretreatment apparent diffusion coefficients. *AJR Am J Roentgenol* 2007;188:1001–8.
 21. Liapi E, Geschwind JF, Vossen JA, et al. Functional MRI evaluation of tumor response in patients with neuroendocrine hepatic metastasis treated with transcatheter arterial chemoembolization. *AJR Am J Roentgenol* 2008;190:67–73.
 22. Nasu K, Kuroki Y, Nawano S, et al. Hepatic metastases: diffusion weighted sensitivity-encoding versus SPIO-enhanced MR imaging. *Radiology* 2006;239:122–30.
 23. Parikh T, Drew SJ, Lee VS, et al. Focal liver lesion detection and characterization with diffusion-weighted MR imaging: comparison with standard breath-hold T2-weighted imaging. *Radiology* 2008;246:812–22.
 24. Ries M, Jones RA, Basseau F, et al. Diffusion tensor MRI of the human kidney. *J Magn Reson Imaging* 2001;14:42–9.
 25. Squillaci E, Manenti G, Cova M, et al. Correlation of diffusion-weighted MR imaging with cellularity of renal tumours. *Anticancer Res* 2004;24:4175–9.
 26. Cova M, Squillaci E, Stacul F, et al. Diffusion-weighted MRI in the evaluation of renal lesions: preliminary results. *Br J Radiol* 2004;77:851–7.
 27. Chan JH, Tsui EY, Luk SH, et al. MR diffusion-weighted imaging of kidney: differentiation between hydronephrosis and pyonephrosis. *Clin Imaging* 2001;25:110–3.
 28. Namimoto T, Yamashita Y, Mitsuzaki K, et al. Measurement of the apparent diffusion coefficient in diffuse renal disease by diffusion-weighted echo-planar MR imaging. *J Magn Reson Imaging* 1999;9:832–7.
 29. Fukuda Y, Ohashi I, Hanafusa K, et al. Anisotropic diffusion in kidney: apparent diffusion coefficient measurements for clinical use. *J Magn Reson Imaging* 2000;22:156–60.
 30. Squillaci E, Manenti G, Di Stefano F, et al. Diffusion-weighted MR imaging in the evaluation of renal tumours. *J Exp Clin Cancer Res* 2004;23:39–45.
 31. Hosseinzadeh K, Schwartz SD. Endorectal diffusion-weighted imaging in prostate cancer to differentiate malignant and benign peripheral zone tissue. *J Magn Reson Imaging* 2004;20:654–61.
 32. Issa B. In vivo measurements of the apparent diffusion coefficient in normal and malignant prostatic tissues using echo-planar imaging. *J Magn Reson Imaging* 2002;16:196–200.
 33. Nasu K, Kuroki Y, Kuroki S, et al. Diffusion-weighted single shot Echo planar imaging of colorectal cancer using a sensitivity-encoding technique. *Jpn J Clin Oncol* 2004;34:620–6.
 34. Ichikawa T, Erturk SM, Motosugi U, et al. High-B-value diffusion weighted MRI in colorectal cancer. *AJR Am J Roentgenol* 2006;187:181–4.
 35. Ichikawa T, Erturk SM, Motosugi U, et al. High-b value diffusion-weighted MRI for detecting pancreatic adenocarcinoma: preliminary results. *AJR Am J Roentgenol* 2007;188:409–14.
 36. Fujii S, Matsusue E, Kigawa J, et al. Diagnostic accuracy of the apparent diffusion coefficient in differentiating benign from malignant uterine endometrial cavity lesions: initial results. *Eur Radiol* 2008;18:384–9.
 37. Tamai K, Koyama T, Saga T, et al. Diffusion-weighted MR imaging of uterine endometrial cancer. *J Magn Reson Imaging* 2007;26:682–7.
 38. Naganawa S, Sato C, Kumada H, et al. Apparent diffusion coefficient in cervical cancer of the uterus: comparison with the normal uterine cervix. *Eur Radiol* 2005;15:71–8.
 39. Nakayama T, Yoshimitsu K, Irie H, et al. Diffusion-weighted echo-planar MR imaging and ADC mapping in the differential diagnosis of ovarian cystic masses: usefulness of detecting keratinoid substances in mature cystic teratomas. *J Magn Reson Imaging* 2005;22:271–8.
 40. Fuji S, Matsusue E, Kanasaki Y, et al. Detection of peritoneal dissemination in gynecological malignancy: evaluation by diffusion-weighted MR imaging. *Eur Radiol* 2008;18:18–23.
 41. Matoba M, Tonami H, Kondou T, et al. Lung carcinoma: diffusion-weighted MR imaging—preliminary evaluation with apparent diffusion coefficient. *Radiology* 2007;243:570–7.
 42. Kwee TC, Takahara T, Ochiai R, et al. Diffusion-weighted whole-body imaging with background body signal suppression (DWIBS): features and potential applications in oncology. *Eur Radiol* 2008;18:1937–52.
 43. Ohno Y, Koyama H, Onishi Y, et al. Non-Small cell lung cancer: Whole-body MR examination for M-stage assessment—utility for whole-body diffusion-weighted imaging compared with integrated FDG PET/CT. *Radiology* 2008;248:643–54.
 44. Mürtz P, Krautmacher C, Träber F, et al. Diffusion-weighted whole-body MR imaging with background body signal suppression: a feasibility study at 3.0 Tesla. *Eur Radiol* 2007;17:3031–7.
 45. Komori T, Narabayashi I, Matsumura K, et al. 2-[Fluorine-18]-fluoro-2-deoxy-D-glucose positron

- emission tomography/computed tomography versus whole-body diffusion-weighted MRI for detection of malignant lesions: initial experience. *Ann Nucl Med* 2007;21:209–15.
46. Li S, Sun F, Jin ZY, et al. Whole-body diffusion-weighted imaging: technical improvement and preliminary results. *J Magn Reson Imaging* 2007; 26:1139–44.
 47. Ballon D, Watts R, Dyke JP, et al. Imaging therapeutic response in human bone marrow using rapid whole-body MRI. *Magn Reson Med* 2004;52: 1234–8.
 48. Zhang J, Tehrani YM, Wang L, et al. Renal masses: characterization with diffusion-weighted MR imaging—a preliminary experience. *Radiology* 2008;247:458–64.
 49. Yoshikawa T, Kawamitsu H, Mitchell DG, et al. ADC measurement of abdominal organs and lesions using parallel imaging technique. *AJR* 2006;187: 1521–30.
 50. Chen C-Y, Li C-W, Kuo Y-T, et al. Early response of hepatocellular carcinoma to transcatheter arterial chemoembolization: choline levels and MR diffusion constants—initial experience. *Radiology* 2006;239: 448–56.
 51. Cui Y, Zhang X-P, Sun Y-S, et al. Apparent diffusion coefficient: potential imaging biomarker for prediction and early detection of response to chemotherapy in hepatic metastases. *Radiology* 2008; 248:894–900.
 52. Kamel IR, Bluemke DA, Ramsey D, et al. Role of diffusion-weighted imaging in estimating tumor necrosis after chemoembolization of hepatocellular carcinoma. *AJR* 2003;181:708–10.
 53. Hamstra DA, Rehemtulla A, Ross BD. Diffusion magnetic resonance imaging: a biomarker for treatment response in oncology. *J Clin Oncol* 2007;25:4104–9.
 54. Naganawa S, Sato C, Nakamura T, et al. Diffusion-weighted images of the liver: Comparison of tumor detection before and after contrast enhancement with superparamagnetic iron oxide. *J Magn Reson Imaging* 2005;21:836–40.
 55. Chan JHM, Tsui EYK, Luk SH, et al. Diffusion-weighted MR imaging of the liver: distinguishing hepatic abscess from cystic or necrotic tumor. *Abdom Imaging* 2001;26:161–5.
 56. Sukru M, Erturk SM, Ichikawa T, et al. Diffusion-weighted MR imaging in the evaluation of pancreatic exocrine function before and after secretin stimulation. *Am J Gastroenterol* 2006;101:133–6.
 57. Magnetic resonance imaging of benign spinal lesions simulating metastasis: role of diffusion-weighted imaging. *Top Magn Reson Imaging* 2000;11:224–34.
 58. Tsuchiya K, Katase S, Yoshino A, et al. Diffusion-weighted MR imaging of encephalitis. *Am J Roentgenol* 1999;173:1097–9.
 59. Asao C, Korogic Y, Kitajima M, et al. Diffusion-weighted imaging of radiation-induced brain injury for differentiation from tumor recurrence. *AJNR Am J Neuroradiol* 2005;26:1455–60.